CH-π interaction boosts photocatalytic CO_2 reduction activity in a noble-metal-free system with a molecular cobalt catalyst anchored on carbon nitride

Jia-Wei Wang,[1] Marcos Gil-Sepulcre,[2,3] Hai-Hua Huang,[4] Eduardo Solano,[5] Yan-Fei Mu,[6] Antoni Llobet*[2,3,10], Gangfeng Ouyang*[1,7,8,9]

[1]KLGHEI of Environment and Energy Chemistry, School of Chemistry, Sun Yat-sen University, Guangzhou 510275, China

[2]Institute of Chemical Research of Catalonia (ICIQ), Barcelona Institute of Science and Technology (BIST), 43007 Tarragona, Spain

[3]Departament de Química, Universitat Autònoma de Barcelona, 08193 Barcelona, Spain

[4]School of Materials Science & Engineering, School of Chemistry, PCFM Lab, Sun Yat-sen University, Guangzhou 510275, China

[5]NCD-SWEET beamline, ALBA synchrotron light source. Carrer de la Llum, 2, 26, 08290 Cerdanyola del Vallès, Barcelona

[6]Institute of New Energy Materials and Low Carbon Technology, School of Material Science and Engineering, Tianjin University of Technology, Tianjin 300384, China

[7]Instrumental Analysis and Research Center, Sun Yat-sen University, Guangzhou, 510275, China

[8]Chemistry College, Center of Advanced Analysis and Gene Sequencing, Zhengzhou University, Zhengzhou 450001, China

[9]Guangdong Provincial Key Laboratory of Emergency Test for Dangerous Chemicals, Guangdong Institute of Analysis (China National Analytical Center Guangzhou), Guangzhou, 510070, China

[10]The Lead Contact

*Correspondence: allobet@iciq.cat (A. Llobet); cesoygf@mail.sysu.edu.cn (G. Ouyang)

Summary

The construction of efficient noble-metal-free systems for visible-light-driven CO_2 reduction still remains a key challenge. Here we report an efficient molecular hybrid system composed of a Co-PYN5 catalyst that contains a pyrene functionality that anchors on *g*-C_3N_4 dye surface via CH-π interactions. This hybrid material achieves high TONs and TOFs for visible light reduction of CO_2 to CO of 533 and 95 h^{-1}, that are within the best reported up to now. The exceptional performance is rationalized in terms of the electronic coupling that takes place with the π-system of the pyrene group with both the *g*-C_3N_4 surface and the Co-pyridyl moiety of the catalysts.

Introduction

The light induced transformation of CO_2 into reduced products such as CO, CH_4, MeOH, EtOH or others is of great interest because it can reduce the concentration of CO_2 in the atmosphere and thus mitigate the effects of global warming.[1-3,4,5] Further, CO_2 reduced products can be used as synthons for the chemical industry to generate value-added chemicals.[6-8]

Several first-row transition metal complexes have been identified so far as CO_2 reduction catalysts (CRCs) that are capable of catalytically reducing CO_2 with good efficiencies and certain degree of selectivity, although improvement is still needed to employ them for technological purposes. The well-defined redox properties and mechanistic understanding of molecular catalyst allow to obtain a valuable knowledge of the key factors that govern the overall catalytic performance.[9,10] This in turn is the *sine qua non* condition for the rational design of selective and powerful catalyst based on the molecular toolkit. The versatility of the latter constitutes an excellent platform for the discovery of long lasting, powerful and selective CO_2 reduction catalysts based on a judicious choice of transition metals and ligands.[9,11]

Regarding the light induced reduction of CO_2, many examples described in the literature use precious metals like Re,[12] Ru[13-15] or Ir[8,16] and only a limited number of them utilize organic dyes[17,18] or abundant transition metal complexes[19-21] as catalysts and/or photosensitizers. Recent efforts have been focused on the use of earth-abundant systems,[22-25] but their performances are far from ideal and thus need substantial improvement. In this context, graphitic carbon nitride (*g*-C_3N_4) emerges as a very interesting material, due to its facile synthesis and easily tunable properties.[25-31] Pioneering examples utilize Ru complexes with mesoporous *g*-C_3N_4 (*mpg*-C_3N_4) to achieve visible-light-driven CO_2 reduction to HCOOH with high selectivity[29,30,32,33] and recently, a carbon nitride/Fe-qpy (qpy is 2,2':6',2":6",2"'-quaterpyridine) system was reported to exhibit an impressive TON of 155 and 97% selectivity for the generation of CO.[27]

Several factors are fundamental for the successful accomplishment of light induced CO_2 reduction using solid state molecular hybrid materials. These include the intrinsic capacity of the CO_2 reduction molecular catalyst to effectively and selectively transform CO_2 to CO (or other reduced products) at relatively low overpotentials and the use of a light absorbing material with the right band energies and a sufficiently long charge separation state that can effectively interact with the

molecular catalysts. The nature and degree of the interaction of the material with the molecular catalyst will be determined by the electronic communication between them that in turn will affect the interfacial electron transfer kinetics and therefore is one of the crucial elements for a successful design of a solid-state light induced CO_2 reduction system.[34,35]

In this regard, for the particular case of *g*-C_3N_4, several strategies have been used, including weak van der Waals interactions[27] between molecular catalyst and *g*-C_3N_4 as well as strong covalent amide bonds.[24,36] In the latter case the amide bond is generated between free amine groups at the *g*-C_3N_4 semiconductor and a non-bonding carboxylic group of the ligand bonded to a cobalt center. Further π-π staking interaction have also been used in molecular catalysts by simply adding them on top of the *g*-C_3N_4 surfaces or using a polymerization strategy.[25,31]

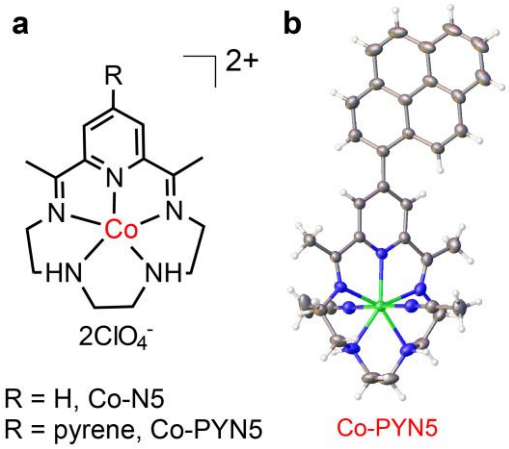

Figure 1. Catalyst structures. (a) Drawn structures for Co-N5 and Co-PYN5. (b) ORTEP plot of the cationic part of the complex $[Co(PYN5)(MeCN)_2](ClO_4)_2$. Color code: Co, green; N, blue; C, gray; H, white. Counter ions have been omitted for clarity.

To this end, we considered the utilization of a novel anchoring methodology based on CH-π interactions[37-40] between the CH-aromatic groups of the ligand and the π-system of *g*-C_3N_4 absorber as a simple strategy to prepare molecular hybrid materials that can potentially accelerate interfacial electron transfer via this type of bonding. For this purpose, we have prepared a Co complex that contains the ligand, (2*E*,12*E*)-2,13-dimethyl-14-(pyren-1-yl)-3,6,9,12-tetraaza-1(2,6)-pyridinacyclotridecaphane-2,12-diene, abbreviated as PYN5. The latter is a pentadentate ligand that occupies the equatorial positions of the Co metal center and that contains a pyrene group appended

into its pyridyl ring, as can be observed in **Figure 1**. Further, the PYN5 ligand coordinates the Co(II) center as a neutral ligand and hence enables the dicationic nature of the Co-PYN5 complex.

Results and discussion

Here on we report the synthesis and characterization of Co-PYN5, its anchoring onto *g*-C_3N_4, as well as the characterization of the new molecular hybrid material, Co-PYN5@*g*-C_3N_4. Further, we describe the performance of Co-PYN5@*g*-C_3N_4 regarding its capacity to catalytically carry out the light induced reduction of CO_2 to CO. The present system displays very high values in terms of both TON (533) and TOF (95 h^{-1}) for photocatalytic CO_2-to-CO conversion with organic absorbers and using first row transition metals as catalysts.

Further, it is the first example of anchoring a molecular catalyst via CH-π interaction for the CO_2 reduction reaction. For comparative purposes the parent Co complex without the appended pyrene group, Co-N5 (N5 is (2*E*,12*E*)-2,13-dimethyl-3,6,9,12-tetraaza-1(2,6)-pyridinacyclotridecaph-ane-2,12-diene; **Figure 1**) was also prepared. The synthesis of Co-N5 consists of a template complexation reaction where 2,6-diacetyl-pyridyl reacts with triethylenetetramine in the presence of Co(II) salts as previously described in the literature.[11] A similar method was used for the synthesis of Co-PYN5 but using the diacetyl reactant functionalized with a pyrene moiety. This generates Co-PYN5 that is highly soluble in MeCN and crystallizes as the $[Co(PYN5)(MeCN)_2](ClO_4)_2$ complex where two solvent molecules coordinate to the Co metal center, as can be observed in the ORTEP structure shown in **Figure 1**. The metal center has a pseudo pentagonal bipyramidal geometry where the PYN5 ligand occupies the equatorial position while the MeCN ligand coordinated at the axial ones. It is interesting to realize here that the equatorial Co-N bonding distances range from 2.19 to 2.27 Å with an average of 2.24 Å. This is 0.30 Å larger than typical Co(II)-N bonds for related complexes such as Co-N4, $[Co(N4)]^{2+}$ (N4 = (2*E*,12*E*)-2,12-dimethyl-3,7,11,17-tetraazabicyclo[11.3.1]hepta-deca-1(17),2,11,13,15-pentaene),[41] which contains a tetradentate equatorial ligand and manifests that in Co-PYN5 the Co-N bonds at the equatorial zone are relatively weak and can synchronically coordinate and decoordinate in order not to violate the 18-electron rule.[11] As a consequence, when one of the aliphatic N of PYN5 is not coordinated, it can also act as a proton acceptor or hydrogen bonding site close to the axial positions where the CO_2 reduction

transformation will occur and therefore can help to significantly reduce the activation energies for the CO_2 reduction reaction as has been recently reported for both reduction and oxidation reactions involving proton transfer steps in the rate determining step.[42,43]

Another interesting feature of the $[Co(PYN5)(MeCN)_2]^{2+}$ structure is the 119.4º dihedral angle between the acetyl and pyrene groups due to the steric hindrance produced by the alpha-CH groups of each moiety. This avoids potential π-π stacking interactions with the graphitic surface but is responsible for its anchoring via the CH-π interaction as will be discussed below.

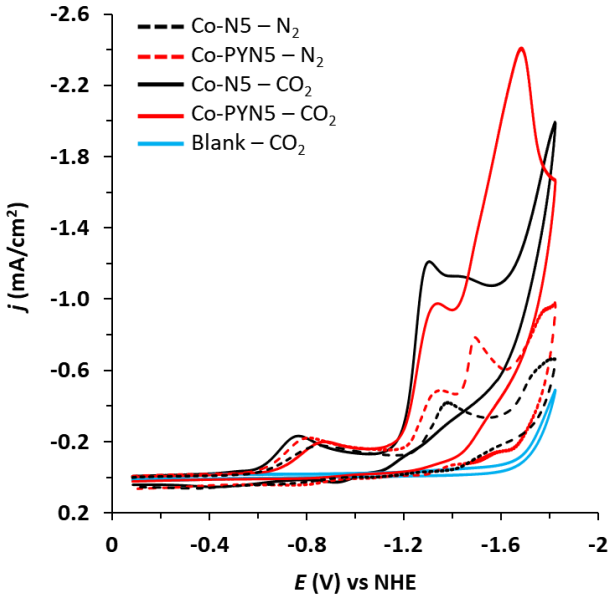

Figure 2. Cyclic voltammetry. Cyclic voltammograms of 1.0 mM Co-N5 (black lines) and Co-PYN5 (red lines) in dry MeCN containing 0.1 M $TBAPF_6$ as supporting electrolyte, under N_2 (dashed lines) and CO_2 (solid lines). Experiments performed using a glassy carbon disk as a working electrode, $Ag/AgNO_3$ (0.01 M $AgNO_3$ in MeCN) as reference electrode and a Pt wire as auxiliary electrode at a scan rate of 100 mV/s. The background current under CO_2 is shown for comparison (cyan).

The electrochemical properties of Co-PYN5 and Co-N5 were investigated based on cyclic voltammetry (CV) experiments in the presence and absence of CO_2 using MeCN as solvent and the results are shown in **Figure 2**. All potentials reported here are measured using ferrocene as an internal standard and transformed to normal hydrogen electrode (NHE) by adding +0.63 V.[14,44] On the cathodic side, in the absence of CO_2 each of the complexes presents a one-electron reduction event in the range of -0.80 to -0.84 V that is associated with the Co(II)L/Co(I)L redox couple, with

an anodic peak at roughly -0.75-0.85 V. Then, in the -1.20 - -1.81 V range Co-N5 presents two redox processes that are associated with two consecutive ligand reductions. The first one at $E_{p,a}$ = -1.37 V (Co(I)L$^{\cdot -}$/Co(I)L) and the second one at $E_{p,a}$ = -1.78 V (Co(I)L$^{\cdot\cdot 2-}$/(Co(I)L$^{\cdot -}$). On the other hand, the Co-PYN5 shows three ligand based redox process, two of them at the same potentials as Co-N5 and an additional wave at $E_{p,a}$ = -1.48 V that can be tentatively assigned to the reduction of the pyrene moiety. In the presence of CO_2, the first Co(II)/Co(I) cathodic wave for either Co-N5 or and Co-PYN5 remains mainly unaltered and a new catalytic wave appears at E_{onset} = -1.15 V, close to the Co(I)L/Co(I)L$^{\cdot -}$ couple, and thus manifesting that the Co(I)L$^{\cdot -}$ species is sufficiently nucleophilic to interact with CO_2 and provokes the catalytic reduction of CO_2. Based on the above results, little difference is revealed for their catalytic activities.

Further for the case of Co-PYN5, a second catalytic wave appears at E_{onset} = -1.43 V that coincides with the pyrene-based reduction mentioned above thanks to a larger degree of π-delocalization. This is interesting because the triply reduced complex in the Co-PYN5 case produces a much more nucleophilic species than the doubly reduced one that will be accessible to the Conduction Band (CB) of the *g*-C_3N_4 absorber.

The CV experiments of Co-PYN5 and Co-N5 were also registered in the presence 5% TFE under CO_2 in MeCN as solvent and are displayed in **Figures S1 and S2**. Interestingly, as can be observed all potentials cathodically shift by about 200 mV and the onset of catalysis now occurs at approx. -1.0 V. Electrocatalytic experiments were carried out by means of bulk electrolysis for both Co-PYN5 and Co-N5 in MeCN with 5% TFE as a proton source at an applied potential of -1.30 V, giving mainly CO and H_2 as products, in ratio of 3.8 and 2.5, respectively (**Table S1**).

As a visible light absorbing material, we used *g*-C_3N_4 obtained from the polymerization of urea as described in the literature.[23] To anchor the catalyst into the light absorbing material we prepared a 5 mM Co catalyst solution in 5 mL of MeCN and added 4 mg of *g*-C_3N_4 powder. Then the mixture was centrifuged and the obtained solid was washed with MeCN and dried at vacuum (see experimental details in the SI).

This generated the hybrid material Co-PYN5@*g*-C_3N_4, where the catalyst is attached to the surface of *g*-C_3N_4. Following the same methodology but using Co-N5 without the pyrene functionality did not generate any anchored catalyst at the surface of *g*-C_3N_4 and thus manifests that the pyrene group is responsible for anchoring at the absorber surface. The absence of Co-N5 at the surface of *g*-C_3N_4

was evidenced by both UV-vis and 2D grazing incidence wide angle X-ray scattering (GIWAXS) analysis that are reported in the SI as **Figures S3 and S4**, respectively. To quantify the amount of Co-PYN5 at the surface we carried out inductively coupled plasma (ICP) analysis that gave a value of 2.14 μmols/g.

The non-planarity of the pyrene and pyridyl rings (119.4º) mentioned previously excludes the possibility of conventional π-π interactions between the pyrene group and the nearly planar structure of *g*-C_3N_4. This leaves CH-π interactions as the only possible bond besides potential van der Waals interactions. This was further confirmed by DFT calculations where we used a continuous VASP model to simulate the *g*-C_3N_4 surface and using [Co(PYN5)Cl]Cl as a model complex. The results obtained can be graphically observed in **Figure 3** where the pyrene group is positioned perpendicular to the *g*-C_3N_4 surface with two CH groups pointing close to the center of the C_3N_3 hexagonal ring and thus maximizing the interactions. The distances between the CH group and the plane defined by the C_3N_3 ring are 2.13 Å and 2.69 Å, respectively. The calculated adsorption energy is of 11.2 kcal/mol that corresponds to an average of 5.6 kcal/mol per CH-π interaction that is in agreement with those previously reported data.[38,40,45,46] An electronic density map of the interaction between the *g*-C_3N_4 surface and the pyrene group of the Co-PYN5 catalyst is provided in the SI (**Figure S5**).

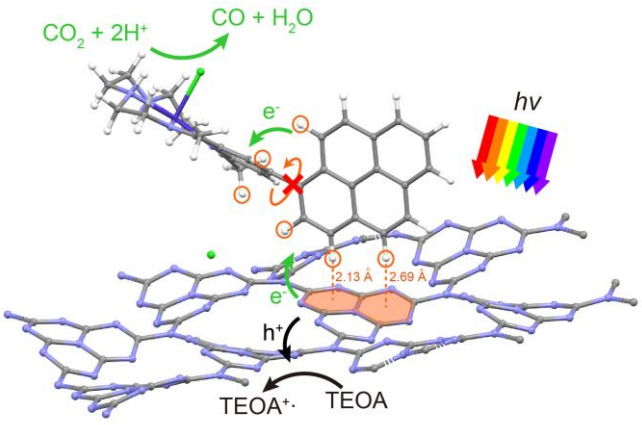

Figure 3. DFT calculation. Drawn structure for the Co-PYN5@*g*-C_3N_4 molecular hybrid material based on DFT calculations. The CH-π interaction and distances between Co-PYN5 and *g*-C_3N_4, are shown with orange dashed lines while the electron-hole flow during the light induced CO_2 reduction catalysis is indicated with green and black arrows respectively.

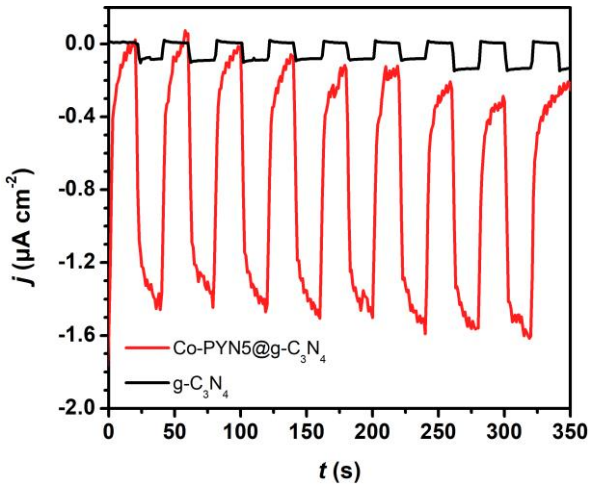

Figure 4. Photocurrent measurements. Transient (light on/off) photocurrent responses of *g*-C_3N_4 (black), Co-PYN5@*g*-C_3N_4 (red) hybrid ink dropped onto an FTO electrode (no bias, 0.5 M $NaClO_4$ solution).

The new hybrid material was further characterized by powder X-ray diffraction (PXRD; **Figure S6**), diffuse reflectance spectroscopy (DRS; **Figure S7**) and X-ray photoelectron spectroscopy (XPS; **Figure S8**) and these results are displayed in the SI. The light absorbing properties of the hybrid material were also characterized based on fluorescence and time-resolved photoluminescence (TRPL) spectroscopy on solid samples (**Figures S9 and S10**). Further photocurrent responses were also measured on FTO electrodes (**Figure 4**).

The fluorescence spectra of *g*-C_3N_4 show typical emission band at 433 nm.[23] In the presence of either TEOA or Co-PYN5 the emission is partially quenched. Interestingly, when a combination of TEOA and Co-PYN5 is added, the emission is quenched to a larger extend consistent with the electron donating capacity of the TEOA to react with the hole generated upon illumination of the *g*-C_3N_4 material and the corresponding reduction of Co(II) to Co(I) by the excited electrons on the CB. A related phenomenon is observed by TRPL with a lifetime of 7.55 ns for *g*-C_3N_4 that agrees with previous examples reported in the literature.[47] In the presence of Co-PYN5 and TEOA, there is a significant lifetime reduction that is even more pronounced when both TEOA and Co-PYN5 are present at the same time till 5.40 ns (See detailed information in the SI). Interestingly, bias-free transient (light on/off) photocurrent responses of 0.1 μA/cm^2 for *g*-C_3N_4@FTO in a 0.5 M $NaClO_4$ aqueous solution are observed (**Figure 4**). In the presence of the Co catalyst under the same

conditions the photocurrent response obtained for Co-PYN5@*g*-C_3N_4@FTO increases 15 times up to 1.5 μA/cm^2 with practically no attenuation after 8 consecutive illumination cycles.

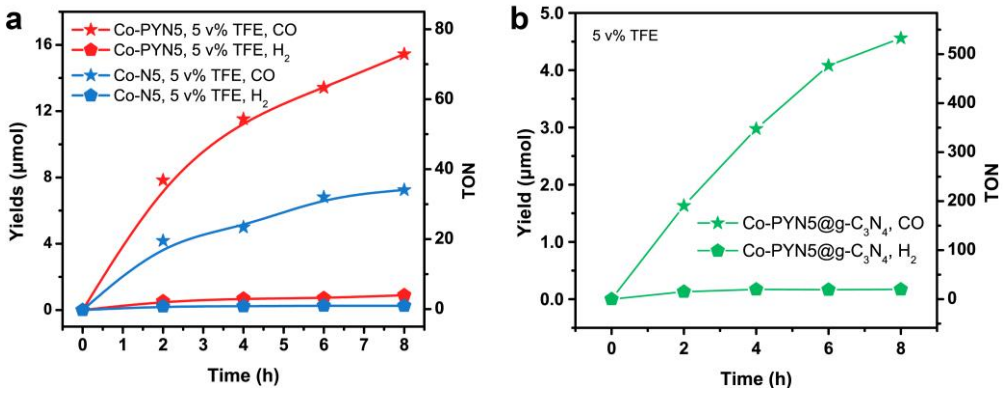

Figure 5. **Photocatalytic CO_2 reduction.** (a) Time profiles of photocatalytic CO (star) and H_2 (pentagon) formation from a MeCN/TEOA (v:v = 4:1) solution containing 4.0 mg *g*-C_3N_4, 5 v% TFE and 50 μM Co-PYN5 (red) or Co-N5 (blue). (b) Time profiles of photocatalytic CO (star) and H_2 (pentagon) formation from a CH_2Cl_2/TEOA (v:v = 4:1) solution containing 4.0 mg Co-PYN5@*g*-C_3N_4 and 5 v% TFE.

Photocatalytic experiments for the reduction of CO_2 were carried out using the hybrid material Co-PYN5@*g*-C_3N_4 in a home-made quartz vessel with triethanolamine as a sacrificial electron donor, TFE as proton source and a mercury lamp ($\lambda \geq 400$ nm) as the light source under 1 atm pressure of CO_2. Initially the experiments were carried out by adding *g*-C_3N_4 (1 g/L) into a MeCN/TEOA (v:v = 4:1) solution containing the Co catalyst. CO was the main product observed. Using labelled $^{13}CO_2$ allows to confirm that the generated CO comes exclusively from CO_2 (**Figure S11**).

A typical time profile of [Co-PYN5+*g*-C_3N_4] system for photocatalytic CO_2 reduction is displayed in **Figure 5**. Using a [Co-PYN5] of 50 μM and after 8 h of irradiation, 15.4 μmol of CO was detected as the dominant gaseous product, consistent with a 94% CO selectivity and a turnover number (TON) of 77 (**Table 1**, entry 2). This is in sharp contrast with the electrocatalytic conditions described earlier in homogeneous phase where the CO selectivity is significantly lower. For the Co-N5 catalyst, in the absence of the pyrene group, the species absorbed or in close contact with the surface drastically decreases, giving a TON of 37, which is 2 times lower as compared to the Co-PYN5 in the same conditions (**Table 1**, entry 5). This comparison clearly manifests that the CH-π interaction

significantly promotes the photocatalytic performance. The increased reactivity of the Co-PYN5 versus Co-N5 can also be observed under the same conditions as previously described but in the absence of TFE, see entries 1 and 4 in **Table 1**, where the reactivity of the pyrene containing complex is 5 times higher toward the formation of CO.

Given the high solubility of the catalysts in MeCN, an equilibrium between catalyst and *g*-C_3N_4 material is established in this solvent, as indicated in the equation below,

g-C_3N_4 (s) + Co-PYN5 (dis) $\rightleftharpoons$ Co-PYN5@*g*-C_3N_4 (s) (1)

Consequently, only the adsorbed catalytic species, Co-PYN5@*g*-C_3N_4, will be active and thus the TON reported here represents a lower limit of the catalyst performance.

Table 1. Photocatalytic reduction of CO_2 to CO by cobalt complexes and comparison with reported results for CO_2 reduction to CO in MeCN/TEOA with *g*-C_3N_4.

Entry	**[Catalyst]**	**[Absorber]**	**Light source**	**QE (%)**	**CO (µmol)**	**H_2 (µmol)**	**CO (%)**	**TON (TOF_i; h^{-1})**	**Time (h)**	**Ref.**
1	Co-PYN5 (50 µM)	*g*-C_3N_4 (1 g/L)	Hg lamp (> 400 nm, 180 mW/cm^2)	0.25 (405 nm)	11.1	0.75	94	55.5	8	tw
2[a]	Co-PYN5 (50 µM)	*g*-C_3N_4 (1 g/L)	Hg lamp (> 400 nm, 180 mW/cm^2)	0.45 (405 nm)	15.4	0.89	94	77	8	tw
3[b]	Co-PYN5@*g*-C_3N_4 (2.14 µmol/g)	*g*-C_3N_4 (1 g/L)	Hg lamp (> 400 nm, 180 mW/cm^2)	N.A.	4.56	0.17	96	533 (95)	8	tw
4	Co-N5 (50 µM)	*g*-C_3N_4 (1 g/L)	Hg lamp (> 400 nm, 180 mW/cm^2)	N.A.	2.10	1.14	65	11	8	tw
5[a]	Co-N5 (50 µM)	*g*-C_3N_4 (1 g/L)	Hg lamp (> 400 nm, 180 mW/cm^2)	N.A.	7.25	1.25	85	37	8	tw
6[c]	Co-PYN5 (50 µM)	*g*-C_3N_4 (1 g/L)	Hg lamp (> 400 nm, 180 mW/cm^2)	N.A.	6.70	1.30	84	33.5	8	tw
7	No Cat	*g*-C_3N_4 (1 g/L)	Hg lamp (> 400 nm, 180 mW/cm^2)	N.A.	0.3	0.32	/	/	8	tw

8	Fe(qpy) (20 μM)	*mpg*-C_3N_4 (2 g/L)	Hg lamp (400 W, > 400 nm)	4.2 (> 400 nm)	12.4	0.1	97	155 (50)	17	27
9	Co(Por) (2.2 mg)	*g*-C_3N_4 (10 g/L)	Xe lamp (300 W, > 420 nm)	0.8 (420 nm)	~6	~1.5	80	<1	7	24
10[d]	Fe(TCPP) (0.5 mg)	*g*-C_3N_4 (2 g/L)	Xe lamp (> 420 nm, 220 mW/cm^2)	N.A.	0.7	0	~100%	5.8 (1)	6	25
11	Co(PPc)	*mpg*-C_3N_4 (0.6 g/L)	Xe lamp (> 400 nm, 100 mW/cm^2)	0.03 (400 nm)	2.0	0.35	85	90 (1.8)	48	31
12	Co(qpy) (3 μM)	*mpg*-C_3N_4 (2 g/L)	Xe lamp (> 400 nm, 100 mW/cm^2)	N.A.	0.31	0.04	88%	37	24	36
13	Co(qpy-Ph-COOH) (1.48 μmol/g)	*mpg*-C_3N_4 (2 g/L)	Xe lamp (> 400 nm, 100 mW/cm^2)	0.25 (> 400 nm)	2.28	0.07	97%	254 (6)	96	
14[e]	Co(qpy-NH_2) (15 μM)	graphene acid (0.067 g/L)	Xe lamp (> 400 nm, 100 mW/cm^2)	0.57 (> 400 nm)	7.6	0.27	97%	513 (2.3)	222	21

[a] Addition of 5 v% TFE.

[b] 4 mL CH_2Cl_2/TEOA (4:1), 5 v% TFE.

[c] 0.1 atm CO_2, 0.9 atm Ar.

[d] MeCN/H_2O/TEOA = 3:1:1

[e] 0.05 M BIH, 0.1 M PhOH.

*TCPP = tetra(4-carboxyphenyl)porphyrin; Por = 3,3'-(8,13-diacetyl-3,7,12,17-tetramethylporphyrin-2,18-diyl)dipropionic acid; PPc = polyphthalocyanine; qpy-Ph-COOH = 4-([2,2':6',2":6",2"'-quaterpyridin]-4-yl)benzoic acid, qpy-NH_2 = 4-([2,2':6',2":6",2"'-quaterpyridin]-4-yl)phenylamine.

Further, in order to decouple the equilibrium indicated in **Equation 1**, the photocatalytic experiments were carried out using CH_2Cl_2 as the solvent instead of MeCN, where Co-PYN5 is insoluble. In this case we used the hybrid material Co-PYN5@*g*-C_3N_4 suspended in a CH_2Cl_2 solution in the presence of TEOA under the same conditions. A TON of 533 is reached that is nearly an order of magnitude larger than that in MeCN (**Table 1**, entry 3) and is among the largest reported

in the literature for related systems with no noble metals. Further, an initial turnover frequency (TOF_i; measured during the first two hours) of 95 h^{-1} is obtained that is among the fastest reported in light induced CO_2 reduction systems using non-noble-metal molecular catalysts and *g*-C_3N_4. For comparative purposes, the performances of other relevant molecular catalysts using *g*-C_3N_4 as a light absorber are presented in entries 8-13, **Table 1**, where the interactions with the catalysts and the *g*-C_3N_4 semiconductors are based on van der Waals interaction (entry 8 and 12), π-π stacking (entries 10, 11) and covalent amide bonds (entries 9, 13). Finally, another feature of our system is that it is also active at [CO_2] as low as 0.1 atm as indicated in the entry 6 of Table 1. This is interesting because in fuel, oil and coal combustion the flue gas [CO_2] in dry exhaust gas, is within 10-15% by volume.[48]

Conclusion

Overall, the results presented here prove that the CH-π interaction between molecular Co catalysts and the *g*-C_3N_4 surface provides the ideal electronic interaction for a successful electronic communication between the catalyst and the light absorber. **Figure 6** exhibits an energy diagram containing the main reactions involved, whereas **Figure 3** shows a diagram of the electron and hole flow upon illumination. Visible light irradiation of the *g*-C_3N_4 surface produce a relatively long-lived charge-separated excited state (in the ranges of ns) where the positive charge generated at the VB is quenched by excess TEOA that acts a sacrificial electron donor. On the other hand, the electrons at the CB are collected by the molecular Co(II) catalyst undergoing two consecutive reduction events that provoke the transformation of CO_2 into CO, in agreement with the electrochemical results described earlier (**Figure 2**).

In conclusion, we present a very efficient molecular hybrid system composed of *g*-C_3N_4 semiconductor and a Co-PYN5 catalyst that contains a pyrene functionality and a protonated site ready for potential intramolecular proton transfer and/or hydrogen bonding. The pyrene moiety acts as an anchoring group that adsorbs the Co-PYN5 complex at the surface of the *g*-C_3N_4 dye via CH-π interaction. As consequence of this, the Co concentration at the surface of g-C_3N_4 is much larger for the Co-PYN5 that contains the pyrene group than for Co-N5 that lacks it under similar conditions. In addition, the hybrid system has the right electronic coupling between the pyrene group and the surface thus providing a low energy pathway for interfacial electron transfer (**Figure S1**).

Further the delocalized π-system of pyrene interacts with the π-system of the pyridyl group so that it provides a low energy access to the doubly reduced ligand and the right energy to interact with the CB of g-C_3N_4. This in turn increases the nucleophilicity of the Co complex, making it much more reactive to atmospheric CO_2.

Overall, the understanding ligand effects that include the first and second coordination effects and ligand-based electron transfer capabilities allow to design powerful and selective systems for light induced CO_2 reduction catalysis with non-noble metals involved.

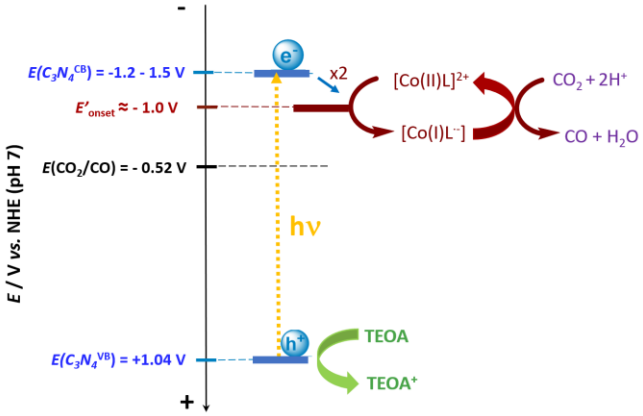

Figure 6. **Reaction diagram.** Simplified energy and reaction scheme proposed to operate in the visible light induced CO_2 reduction to CO by the molecular hybrid material Co-PYN5@g-C_3N_4, in the presence of TEOA as a sacrificial electron donor.

EXPERIMENTAL PROCEDURES

Resource Availability

Lead contact

Further information and requests for resources should be directed to and will be fulfilled by the lead contact, Antoni Llobet (allobet@iciq.cat).

Materials availability

This study generates 4-(pyren-1-yl)-2,6-diacetpypyridine, Co-PYN5 and Co-PYN5@g-C_3N_4 as the new reagents which were obtained by the synthetic procedures below.

Data and code availability

All data needed to support the conclusions of this manuscript are included in the main text or the supplemental information.

Synthesis of 4-(pyren-1-yl)-2,6-diacetpypyridine.

The pyrene-appended compound was prepared by using a modified Suzuki coupling method,[49] where 2.5 mmol of 4-bromo-2,6-diacetpypyridine, 2.5 mmol of pyrene-1-boronic acid, 7.5 mmol of K_2CO_3, 0.25 mmol of $Pd(PPh_3)_4$ and a magnetic stirrer were mixed in a 100 mL Schlenk flask, followed by degassing and purging with nitrogen. At the same time, 10 mL of distilled water and 40 mL of THF was also bubbled with nitrogen under stirring for 30 min, then added to the above Schlenk flask. The reaction mixture was left for 1 day at 75 °C, during which yellow solids were generated. Afterwards, ice cool distilled water was added and the mixture was extracted with 4 × 25 mL of CH_2Cl_2. After evaporation of the solvent, the solid was purified by liquid chromatography. Silica was used as stationary phase. A mixture of petroleum ether/CH_2Cl_2 = 9:1 was used as mobile phase at the initial stage, and turned to pure CH_2Cl_2 to get the second crop of eluent. Elemental analysis ($C_{25}NO_2H_{17}$): Calculated value: C, 82.63; H, 4.72; N, 3.85; Measured value: C, 82.19; H, 4.75; N, 3.70. ESI-MS(+): Calculated for 4-(pyren-1-yl)-2,6-diacetpypyridine ($[M + H]^+$, $C_{25}H_{18}NO_2$) m/z = 364.4, found m/z = 364.4. ^{1}H NMR (400 MHz, Chloroform-*d*) δ 8.54 (s, 2H), 8.29-7.96 (m, 9H), 2.93 (s, 6H).

Synthesis of Co-PYN5.

A sample of 363 mg (1 mmol) of 4-(pyren-1-yl)-2,6-diacetpypyridine and 178 mg (0.5 mmol) of $Co(CF_3SO_3)_2$ were dissolved in 40 mL of toluene/MeCN (v:v = 1:1) at 100 °C under a nitrogen atmosphere. Then, 73 mg (1 mmol) of triethylenetetramine and 0.5 mL anhydrous acetic acid were drop-wise injected into the system, respectively. After 6 h reaction, the solution was cooled to room temperature, dried in vacuum, re-dissolved by adding 50 mL dry CH_3OH and filtrated to remove the unreacted reagents. The filtrate was added with 1 g $NaClO_4$ (excess) to precipitate Co-PYN5 as the brown solids, which was isolated by filtration and rinsing with cold alcohol. The single crystals of Co-PYN5 were obtained by liquid diffusion of ether into the concentrated MeCN solution of Co-PYN5. Yield: 205 mg (56 %). Elemental analysis ($CoC_{31}H_{31}N_5O_8Cl_2$): Calculated value: C, 50.90;

H, 4.27; N, 9.57; Measured value: C, 51.02; H, 4.18; N, 9.50. ESI-MS(+): Calculated for $[Co(PYN5)]^{2+}$ ($[M/2]^{+}$, $C_{15.5}H_{15.5}Co_{1/2}N_{2.5}$) m/z = 266.2, found m/z = 266.2.

Preparation of Co-PYN5@*g*-C_3N_4.

20.0 mg of *g*-C_3N_4, 250 μL of 5 mM Co-PYN5 MeCN solution and 2.0 mL of MeCN were mixed and stirred for 2 h, followed by centrifugation and washing with MeCN twice, dried under vacuum. The Co content of Co-PYN5@*g*-C_3N_4 is estimated as 2.14 ± 0.02 μmol/g (where μmol/g is μmol of Co-PYN5 per gram of Co-PYN5@*g*-C_3N_4) by ICP-MS.

SUPPLEMENTAL INFORMATION

Supplemental Information containing experimental details, supporting figures, and calculation data can be found online.

ACKNOWLEDGMENTS

G. O. thanks the financial support from National Natural Science Foundation of China (21737006, 22076222 and 22036003). J.-W. Wang are grateful for the support from Guangdong Basic and Applied Basic Research Foundation (2020A1515110017 and 2021A1515012033), China Postdoctoral Science Foundation (2020M683020 and 2021T140759) and the Fundamental Research Funds for the Central Universities (20lgpy87). A. L. acknowledges support from Ministerio de Ciencia e Innovación, FEDER and AGAUR through grants: PID2019-111617RB-I00, SO-CEX2019-000925-S and 2017-SGR-1631. We also thank the GIWAXS experiments performed at NCD-SWEET beamline at ALBA synchrotron with the collaboration of ALBA staff (proposal 2020094629).

AUTHOR CONTRIBUTIONS

J.W.W and A.L conceived the idea, designed the experiments and wrote the manuscript. M.G.S performed characterization and wrote the manuscript. H.H.H operated the DFT calculation. E.S carried out the synchrotron experiments. Y.F.M performed the fluorescent experiments. G.O. participated in the discussion and supervised the experiments.

DECLARATION OF INTERESTS

The authors declare no competing interests.

REFERENCES

1. Liu, Z., Guan, D., Wei, W., Davis, S.J., Ciais, P., Bai, J., Peng, S., Zhang, Q., Hubacek, K., Marland, G., et al. (2015). Reduced carbon emission estimates from fossil fuel combustion and cement production in China. Nature *524*, 335-338. 10.1038/nature14677.
2. Tackett, B.M., Gomez, E., and Chen, J.G. (2019). Net reduction of CO_2 via its thermocatalytic and electrocatalytic transformation reactions in standard and hybrid processes. Nat. Catal. *2*, 381-386. 10.1038/s41929-019-0266-y.
3. Xia, C., Zhu, P., Jiang, Q., Pan, Y., Liang, W., Stavitsk, E., Alshareef, H.N., and Wang, H. (2019). Continuous production of pure liquid fuel solutions via electrocatalytic CO_2 reduction using solid-electrolyte devices. Nat. Energy *4*, 776-785. 10.1038/s41560-019-0451-x.
4. Matheu, R., Ertem, M.Z., Gimbert-Surinach, C., Sala, X., and Llobet, A. (2019). Seven Coordinated Molecular Ruthenium-Water Oxidation Catalysts: A Coordination Chemistry Journey. Chem. Rev. *119*, 3453-3471. 10.1021/acs.chemrev.8b00537.
5. Dalle, K.E., Warnan, J., Leung, J.J., Reuillard, B., Karmel, I.S., and Reisner, E. (2019). Electro- and Solar-Driven Fuel Synthesis with First Row Transition Metal Complexes. Chem. Rev. *119*, 2752-2875. 10.1021/acs.chemrev.8b00392.
6. Wu, Y., Jiang, Z., Lu, X., Liang, Y., and Wang, H. (2019). Domino electroreduction of CO_2 to methanol on a molecular catalyst. Nature *575*, 639-642. 10.1038/s41586-019-1760-8.
7. Li, X., Sun, Y., Xu, J., Shao, Y., Wu, J., Xu, X., Pan, Y., Ju, H., Zhu, J., and Xie, Y. (2019). Selective visible-light-driven photocatalytic CO_2 reduction to CH_4 mediated by atomically thin $CuIn_5S_8$ layers. Nat. Energy *4*, 690-699. 10.1038/s41560-019-0431-1.
8. Rao, H., Schmidt, L.C., Bonin, J., and Robert, M. (2017). Visible-light-driven methane formation from CO_2 with a molecular iron catalyst. Nature *548*, 74-77. 10.1038/nature23016.
9. Wang, J.-W., Zhong, D.-C., and Lu, T.-B. (2018). Artificial photosynthesis: Catalytic water oxidation and CO_2 reduction by dinuclear non-noble-metal molecular catalysts. Coord. Chem. Rev. *377*, 225-236. 10.1016/j.ccr.2018.09.003.

10. Wang, J.W., Liu, W.J., Zhong, D.C., and Lu, T.B. (2019). Nickel complexes as molecular catalysts for water splitting and CO_2 reduction. Coord. Chem. Rev. *378*, 237-261. 10.1016/j.ccr.2017.12.009.
11. Wang, J.-W., Yamauchi, K., Huang, H.-H., Sun, J.-K., Luo, Z.-M., Zhong, D.-C., Lu, T.-B., and Sakai, K. (2019). A Molecular Cobalt Hydrogen Evolution Catalyst Showing High Activity and Outstanding Tolerance to CO and O_2. Angew. Chem. Int. Ed. *58*, 10923-10927. 10.1002/anie.201904578.
12. Morimoto, T., Nishiura, C., Tanaka, M., Rohacova, J., Nakagawa, Y., Funada, Y., Koike, K., Yamamoto, Y., Shishido, S., Kojima, T., et al. (2013). Ring-shaped Re(I) multinuclear complexes with unique photofunctional properties. J. Am. Chem. Soc. *135*, 13266-13269. 10.1021/ja406144h.
13. Ouyang, T., Wang, H.-J., Huang, H.-H., Wang, J.-W., Guo, S., Liu, W.-J., Zhong, D.-C., and Lu, T.-B. (2018). Dinuclear Metal Synergistic Catalysis Boosts Photochemical CO_2-to-CO Conversion. Angew. Chem. Int. Ed. *57*, 16480-16485. 10.1002/anie.201811010.
14. Wang, J.-W., Huang, H.-H., Sun, J.-K., Ouyang, T., Zhong, D.-C., and Lu, T.-B. (2018). Electrocatalytic and Photocatalytic Reduction of CO_2 to CO by Cobalt(II) Tripodal Complexes: Low Overpotentials, High Efficiency and Selectivity. ChemSusChem *11*, 1025-1031. 10.1002/cssc.201702280.
15. Wang, J.-W., Qiao, L.-Z., Nie, H.-D., Huang, H.-H., Li, Y., Yao, S., Liu, M., Zhang, Z.-M., Kang, Z.-H., and Lu, T.-B. (2021). Facile electron delivery from graphene template to ultrathin metal-organic layers for boosting CO_2 photoreduction. Nat. Commun. *12*, 813. 10.1038/s41467-021-21084-9.
16. Wang, J.-W., Jiang, L., Huang, H.-H., Han, Z., and Ouyang, G. (2021). Rapid electron transfer via dynamic coordinative interaction boosts quantum efficiency for photocatalytic CO_2 reduction. Nat. Commun. 10.1038/s41467-021-24647-y.
17. Bonin, J., Robert, M., and Routier, M. (2014). Selective and efficient photocatalytic CO_2 reduction to CO using visible light and an iron-based homogeneous catalyst. J. Am. Chem. Soc. *136*, 16768-16771. 10.1021/ja510290t.
18. Rao, H., Bonin, J., and Robert, M. (2017). Visible-light Homogeneous Photocatalytic Conversion of CO_2 into CO in Aqueous Solutions with an Iron Catalyst. ChemSusChem *10*, 4447-4450. 10.1002/cssc.201701467.
19. Takeda, H., Ohashi, K., Sekine, A., and Ishitani, O. (2016). Photocatalytic CO_2 Reduction Using Cu(I) Photosensitizers with a Fe(II) Catalyst. J. Am. Chem. Soc. *138*, 4354-4357. 10.1021/jacs.6b01970.
20. Chen, Z., Hu, Y., Wang, J., Shen, Q., Zhang, Y., Ding, C., Bai, Y., Jiang, G., Li, Z., and Gaponik, N. (2020). Boosting Photocatalytic CO_2 Reduction on $CsPbBr_3$ Perovskite Nanocrystals by Immobilizing Metal Complexes. Chem. Mater. *32*, 1517-1525. 10.1021/acs.chemmater.9b04582.
21. Ma, B., Blanco, M., Calvillo, L., Chen, L., Chen, G., Lau, T.C., Drazic, G., Bonin, J., Robert, M., and Granozzi, G. (2021). Hybridization of Molecular and Graphene Materials for CO_2 Photocatalytic Reduction with Selectivity Control. J. Am. Chem. Soc. *143*, 8414-8425. 10.1021/jacs.1c02250.
22. Lin, J., Pan, Z., and Wang, X. (2013). Photochemical Reduction of CO_2 by Graphitic Carbon Nitride Polymers. ACS Sustainable Chem. Eng. *2*, 353-358. 10.1021/sc4004295.

23. Tang, S., Yin, X., Wang, G., Lu, X., and Lu, T. (2018). Single titanium-oxide species implanted in 2D *g*-C_3N_4 matrix as a highly efficient visible-light CO_2 reduction photocatalyst. Nano Res. *12*, 457-462. 10.1007/s12274-018-2240-4.
24. Zhao, G., Pang, H., Liu, G., Li, P., Liu, H., Zhang, H., Shi, L., and Ye, J. (2017). Co-porphyrin/carbon nitride hybrids for improved photocatalytic CO_2 reduction under visible light. Appl. Catal. B-Environ *200*, 141-149. 10.1016/j.apcatb.2016.06.074.
25. Lin, L., Hou, C., Zhang, X., Wang, Y., Chen, Y., and He, T. (2018). Highly efficient visible-light driven photocatalytic reduction of CO_2 over *g*-C_3N_4 nanosheets/tetra(4-carboxyphenyl)porphyrin iron(III) chloride heterogeneous catalysts. Appl. Catal. B-Environ *221*, 312-319. 10.1016/j.apcatb.2017.09.033.
26. Goettmann, F., Fischer, A., Antonietti, M., and Thomas, A. (2006). Chemical synthesis of mesoporous carbon nitrides using hard templates and their use as a metal-free catalyst for Friedel-Crafts reaction of benzene. Angew. Chem. Int. Ed. *45*, 4467-4471. 10.1002/anie.200600412.
27. Cometto, C., Kuriki, R., Chen, L., Maeda, K., Lau, T.C., Ishitani, O., and Robert, M. (2018). A Carbon Nitride/Fe Quaterpyridine Catalytic System for Photostimulated CO_2-to-CO Conversion with Visible Light. J. Am. Chem. Soc. *140*, 7437-7440. 10.1021/jacs.8b04007.
28. Guo, Z., Chen, G., Cometto, C., Ma, B., Zhao, H., Groizard, T., Chen, L., Fan, H., Man, W.-L., Yiu, S.-M., et al. (2019). Selectivity control of CO versus $HCOO^-$ production in the visible-light-driven catalytic reduction of CO_2 with two cooperative metal sites. Nat. Catal. *2*, 801-808. 10.1038/s41929-019-0331-6.
29. Kuriki, R., Matsunaga, H., Nakashima, T., Wada, K., Yamakata, A., Ishitani, O., and Maeda, K. (2016). Nature-Inspired, Highly Durable CO_2 Reduction System Consisting of a Binuclear Ruthenium(II) Complex and an Organic Semiconductor Using Visible Light. J. Am. Chem. Soc. *138*, 5159-5170. 10.1021/jacs.6b01997.
30. Maeda, K., Kuriki, R., Zhang, M., Wang, X., and Ishitani, O. (2014). The effect of the pore-wall structure of carbon nitride on photocatalytic CO_2 reduction under visible light. J. Mater. Chem. A *2*, 15146-15151. 10.1039/c4ta03128h.
31. Roy, S., and Reisner, E. (2019). Visible-Light-Driven CO_2 Reduction by Mesoporous Carbon Nitride Modified with Polymeric Cobalt Phthalocyanine. Angew. Chem. Int. Ed. *58*, 12180-12184. 10.1002/anie.201907082.
32. Kuriki, R., Sekizawa, K., Ishitani, O., and Maeda, K. (2015). Visible-light-driven CO_2 reduction with carbon nitride: enhancing the activity of ruthenium catalysts. Angew. Chem. Int. Ed. *54*, 2406-2409. 10.1002/anie.201411170.
33. Kuriki, R., Yamamoto, M., Higuchi, K., Yamamoto, Y., Akatsuka, M., Lu, D., Yagi, S., Yoshida, T., Ishitani, O., and Maeda, K. (2017). Robust Binding between Carbon Nitride Nanosheets and a Binuclear Ruthenium(II) Complex Enabling Durable, Selective CO_2 Reduction under Visible Light in Aqueous Solution. Angew. Chem. Int. Ed. *56*, 4867-4871. 10.1002/anie.201701627.
34. Bi, Q.-Q., Wang, J.-W., Lv, J.-X., Wang, J., Zhang, W., and Lu, T.-B. (2018). Selective Photocatalytic CO_2 Reduction in Water by Electrostatic Assembly of CdS Nanocrystals with a Dinuclear Cobalt Catalyst. ACS Catal. *8*, 11815-11821. 10.1021/acscatal.8b03457.

35. Kuehnel, M.F., Orchard, K.L., Dalle, K.E., and Reisner, E. (2017). Selective Photocatalytic CO_2 Reduction in Water through Anchoring of a Molecular Ni Catalyst on CdS Nanocrystals. J. Am. Chem. Soc. *139*, 7217-7223. 10.1021/jacs.7b00369.
36. Ma, B., Chen, G., Fave, C., Chen, L., Kuriki, R., Maeda, K., Ishitani, O., Lau, T.C., Bonin, J., and Robert, M. (2020). Efficient Visible-Light-Driven CO_2 Reduction by a Cobalt Molecular Catalyst Covalently Linked to Mesoporous Carbon Nitride. J. Am. Chem. Soc. *142*, 6188-6195. 10.1021/jacs.9b13930.
37. Yamakawa, M., Yamada, I., and Noyori, R. (2001). CH/π Attraction: The Origin of Enantioselectivity in Transfer Hydrogenation of Aromatic Carbonyl Compounds Catalyzed by Chiralη6-Arene-Ruthenium(II) Complexes. Angew. Chem., Int. Ed. *40*, 2818-2821. 10.1002/1521-3773(20010803)40:15<2818::Aid-anie2818>3.0.Co;2-y.
38. Neel, A.J., Hilton, M.J., Sigman, M.S., and Toste, F.D. (2017). Exploiting non-covalent pi interactions for catalyst design. Nature *543*, 637-646. 10.1038/nature21701.
39. Schindler, D., Gil-Sepulcre, M., Lindner, J.O., Stepanenko, V., Moonshiram, D., Llobet, A., and Würthner, F. (2020). Efficient Electrochemical Water Oxidation by a Trinuclear Ru(bda) Macrocycle Immobilized on Multi-Walled Carbon Nanotube Electrodes. Adv. Energy Mater. *10*, 2002329. 10.1002/aenm.202002329.
40. Hoque, M.A., Gil-Sepulcre, M., de Aguirre, A., Elemans, J., Moonshiram, D., Matheu, R., Shi, Y., Benet-Buchholz, J., Sala, X., Malfois, M., et al. (2020). Water oxidation electrocatalysis using ruthenium coordination oligomers adsorbed on multiwalled carbon nanotubes. Nat. Chem. *12*, 1060-1066. 10.1038/s41557-020-0548-7.
41. Lacy, D.C., McCrory, C.C., and Peters, J.C. (2014). Studies of cobalt-mediated electrocatalytic CO_2 reduction using a redox-active ligand. Inorg. Chem. *53*, 4980-4988. 10.1021/ic403122j.
42. Helm, M.L., Stewart, M.P., Bullock, R.M., DuBois, M.R., and DuBois, D.L. (2011). A synthetic nickel electrocatalyst with a turnover frequency above 100,000 s^{-1} for H_2 production. Science *333*, 863-866. 10.1126/science.1205864.
43. Matheu, R., Ertem, M.Z., Benet-Buchholz, J., Coronado, E., Batista, V.S., Sala, X., and Llobet, A. (2015). Intramolecular Proton Transfer Boosts Water Oxidation Catalyzed by a Ru Complex. J. Am. Chem. Soc. *137*, 10786-10795. 10.1021/jacs.5b06541.
44. Ouyang, T., Huang, H.-H., Wang, J.-W., Zhong, D.-C., and Lu, T.-B. (2017). A Dinuclear Cobalt Cryptate as a Homogeneous Photocatalyst for Highly Selective and Efficient Visible-Light Driven CO_2 Reduction to CO in CH_3CN/H_2O Solution. Angew. Chem. Int. Ed. *56*, 738-743. 10.1002/anie.201610607.
45. Tsuzuki, S., Honda, K., Uchimaru, T., Mikami, M., and Tanabe, K. (2000). Origin of the Attraction and Directionality of the NH/π Interaction: Comparison with OH/π and CH/π Interactions. J. Am. Chem. Soc. *122*, 11450-11458. 10.1021/ja001901a.
46. Plevin, M.J., Bryce, D.L., and Boisbouvier, J. (2010). Direct detection of CH/π interactions in proteins. Nat. Chem. *2*, 466-471. 10.1038/nchem.650.
47. Yang, L., Huang, J., Shi, L., Cao, L., Liu, H., Liu, Y., Li, Y., Song, H., Jie, Y., and Ye, J. (2018). Sb doped SnO_2-decorated porous *g*-C_3N_4 nanosheet heterostructures with enhanced photocatalytic activities under visible light irradiation. Appl. Catal. B-Environ *221*, 670-680. 10.1016/j.apcatb.2017.09.041.

48. Li, X. (2007). Chapter One - Thermodynamic Performance of Fuel Cells and Comparison with Heat Engines. In Advances in Fuel Cells, T.S. Zhao, K.D. Kreuer, and T. Van Nguyen, eds. (Elsevier Science), pp. 1-46. 10.1016/S1752-301X(07)80006-8.

49. Garrido-Barros, P., Gimbert-Surinach, C., Moonshiram, D., Picon, A., Monge, P., Batista, V.S., and Llobet, A. (2017). Electronic pi-Delocalization Boosts Catalytic Water Oxidation by Cu(II) Molecular Catalysts Heterogenized on Graphene Sheets. J. Am. Chem. Soc. *139*, 12907-12910. 10.1021/jacs.7b06828.